Published in final edited form as:
Dev Cell. 2010 September 14; 19(3): 389–401. doi:10.1016/j.devcel.2010.08.004.

Atypical Cadherins Dachsous and Fat Control Dynamics of Noncentrosomal Microtubules in Planar Cell Polarity

Toshiyuki Harumoto[1,2], **Masayoshi Ito**[1,3], **Yuko Shimada**[1,4], **Tetsuya J. Kobayashi**[5,6], **Hiroki R. Ueda**[7], **Bingwei Lu**[8], and **Tadashi Uemura**[1,2]

[1]Graduate School of Biostudies, Kyoto University, Yoshida Konoe-cho, Sakyo-ku, Kyoto 606-8507, Japan

[2]CREST, Japan Science and Technology Agency, Kawaguchi, Saitama 332-0012, Japan

[5]Institute of Industrial Science, the University of Tokyo, 4-6-1 Komaba, Meguro-ku, Tokyo 153-8505, Japan

[6]PRESTO, Japan Science and Technology Agency, Kawaguchi, Saitama 332-0012, Japan

[7]Laboratory for Systems Biology, Center for Developmental Biology, RIKEN, 2-2-3 Minatojima-minamimachi, Chuo-ku, Kobe, Hyogo 650-0047, Japan

[8]Department of Pathology, Stanford University School of Medicine, Stanford, California 94305, USA

Summary

How global organ asymmetry and individual cell polarity are connected to each other is a central question in studying planar cell polarity (PCP). In the Drosophila wing, which develops PCP along its proximal-distal (P-D) axis, we previously proposed that the core PCP mediator Frizzled redistributes distally in a microtubule (MT)-dependent manner. Here we performed organ-wide analysis of MT dynamics by introducing quantitative *in vivo* imaging. We observed MTs aligning along the P-D axis at the onset of redistribution and a small but significant excess of + ends-distal MTs in the proximal region of the wing. This characteristic alignment and asymmetry of MT growth was controlled by atypical cadherins Dachsous (Ds) and Fat (Ft). Furthermore, the action of Ft was mediated in part by PAR-1. All these data support the idea that the active reorientation of MT growth adjusts cell polarity along the organ axis.

Introduction

Cells sense global axes of the tissue to which they belong and manifest polarity for specialized functions. One such example is planar cell polarity (PCP), which is seen in many animals and tissues, such as unidirectionally beating cilia in vertebrate epithelial cells and

Author for correspondence: Tadashi Uemura, Graduate School of Biostudies, Kyoto University, South Campus Research Building, (Building G), Kyoto University, Yoshida Konoe-cho, Sakyo-ku, Kyoto 606-8507, Japan, (Phone) 81-75-753-9238, (Fax) 81-75-753-4265, tauemura@lif.kyoto-u.ac.jp.
[3]Present address: Department of Life Science, Graduate School of Arts and Sciences, the University of Tokyo, 3-8-1 Komaba, Meguro-ku, Tokyo 153-8902, Japan
[4]Present address: Graduate School of Life and Environmental Sciences, University of Tsukuba, Tennoudai 1-1-1, Tsukuba, Ibaraki 305-8572, Japan

epidermal cuticular structures in insects (Adler, 2002; Lawrence, 1966; Wang and Nathans, 2007; Zallen, 2007).

Mechanisms of PCP have been studied in several model systems, and one of them is the Drosophila wing epidermis, which has been investigated with the help of not only molecular genetics but also cell biological methods such as live imaging (Classen et al., 2005; Eaton, 2003; Shimada et al., 2006). In the Drosophila wing, epidermal cells somehow sense the organ cue along the proximal-distal (P-D) axis of the wing, localize an assembly of actin filaments at the distal cell vertex, and generate wing hairs (prehairs) that point distally during pupal development (Figures 1A and 1B).

The pertinent molecular players in the wing, have been classified into at least the 2 following categories: First, atypical cadherins Dachsous (Ds) and Fat (Ft) and the Golgi kinase Four-jointed (Fj) are thought to contribute to the tissue patterning information across the axis (Ma et al., 2003; Matakatsu and Blair, 2004; Simon, 2004; Strutt and Strutt, 2002; Yang et al., 2002). Fj phosphorylates the ectodomains of Ds and Ft, to modulate their bindings; and the phosphorylation of the cytoplasmic domain of Ft is regulated by Ds (Brittle et al., 2010; Feng and Irvine, 2009; Ishikawa et al., 2008; Simon et al., 2010; Sopko et al., 2009). Second, members of the “core group,” including Frizzled (Fz) and the seven-pass transmembrane cadherin Flamingo (Fmi), also known as Starry night (Stan), assemble into asymmetric apicolateral complexes that straddle the proximodistal (P/D) junctions between adjacent cells; and they specify the intracellular location of the wing hair formation by a feedback loop (Figure 1B; Chae et al., 1999; Strutt, 2001; Tree et al., 2002; Usui et al., 1999; Vinson et al., 1989). Just prior to the onset of hair formation, the P/D cell-border localization appears as coherent zigzags that run almost perpendicular to the P-D axis (Figure 1B). When either of the atypical cadherins Ds and Ft does not function, the core members still retain tight localization at selective cell boundaries, but sometimes at wrong boundaries, losing the long-range coordination of the P/D localization (compare Figure 1B with Figure 4B; Ma et al., 2003; Strutt and Strutt, 2002).

In spite of a growing body of information regarding PCP, we are still far from understanding the overall mechanisms underlying it. Outstanding questions include how the above 2 categories of regulators are functionally related to each other at the molecular level (Lawrence et al., 2007; Strutt, 2008; Wu and Mlodzik, 2009), why Fz and Strabismus (Stbm)/Van Gogh (Vang) are localized at distal and proximal cell borders, respectively, in the first place, and how the above core members utilize the cellular machineries to be localized at specialized membrane domains.

The entire pupal development takes about 100 hours. At early stages such as 14 h after puparium formation (APF) or 18 h APF in the region C (see Figure 1A), it was difficult to conclude whether the localization has been already polarized at specific cortexes or not (see Figure 1C). “Interrupted” zigzags start to appear around 24 h APF, and the most coherent zigzags show up at 30 h, just prior to the onset of the hair formation (Figure 1C; Classen et al., 2005; Strutt, 2001; Usui et al., 1999). We have been pursuing the cellular mechanisms that underlie how such a redistribution is achieved. Ultrastructural and immunohistochemical analysis by other groups and us show that (1) non-dividing wing cells have planarly oriented noncentrosomal microtubule (MT) arrays at the level of the adherens junction, and (2) those MTs are approximately aligned along the P-D axis of the wing at 24 h and 30 h APF (Figures 1D and 1E; Eaton et al., 1996; Fristrom and Fristrom, 1975; Shimada et al., 2006; Turner and Adler, 1998). We also performed *in vivo* time-lapse recordings of GFP-tagged Fz mostly in the region C, which demonstrated that Fz-containing vesicles are targeted towards the distal boundaries in a MT-dependent manner. Based on these observations, we have been proposing the “polarized transport” model (Shimada et al.,

2006). Nevertheless at least 2 critical questions have remained to be elucidated: First, how do the MTs become aligned along the P-D axis? Second, why are the Fz vesicles transported distally, but not proximally? One possible scenario may be that + end-distal MTs are more abundant than + end-proximal MTs; in other words, there may be an asymmetry of MT polarity along the P-D axis, which is sufficient to localize the vesicle by a biased random walk (Zimyanin et al., 2008). Our initial analysis of small sampling suggests that there is such an asymmetry (Shimada et al., 2006).

Here we sought more spatiotemporally extensive and quantitative understanding of the growth of the planar MTs in the wing cells of wild-type flies and those of various other genetic backgrounds. In the wild type, growing MTs converged along the P-D axis, which convergence became the most dramatic at 24 h APF. In proximal regions of the wing at this stage, MTs grew in both proximal and distal directions, with a small excess of those with + ends pointing distally. Our data support the possibility that Ds and Ft control both P-D alignment and asymmetry of MT polarity. In our exploring how Ds and Ft control the MT dynamics, we were intrigued by the Ser/Thr kinase PAR-1, whose subcellular localization was controlled at least by Ft. We discussed the possibility that the Ds-Ft system plays a critical role in controlling the dynamics of planar MTs to establish PCP in the Drosophila wing.

Results

Tracking, data collection, and directional analysis of MT growing ends

We visualized growing ends of the planarly oriented MTs by expressing EB1-GFP fusion protein *in vivo*, and tracked the “shooting comet-like” signals by improved time-lapse recordings in the dorsal wing epidermis (Figures 1F and 1G, and Movie S1; see details in Experimental Procedures). Briefly, we tracked over 1,000 comets at each location at a given pupal stage (Figure 1H), measured the angles (from -180° to +180°) of individual comets, and corrected each value with reference to the defined P-D axis of the wing. Then those corrected values were plotted on a Rose diagram to represent the angle distribution and the frequency (Figure 1I; Shindo et al., 2008), thereby allowing us to pursue statistical properties of direction of MT growth, in particular, the directional preference (Figures 1I and 1J; see details in the legends).

Directional distribution of MT growth in the wild type: transient alignment along the P-D axis and local asymmetry of the MT polarity

Spatiotemporal dynamics of MT growth in the wild type were monitored at 4 pupal ages between 14 h APF and 30 h APF, at 4 locations along the P-D axis (Figures 2A, S1A, and S1C; Movies S1 and S2). Those locations belonged to intervein regions in the dorsal wing epidermis and were defined by 4 developing sensory organs as spatial landmarks: 1 on the anterior cross vein (ACV) and the other 3 on the L3 vein (L3-1 to L3-3). It was critical to fix these observation points, because the phenotype of hair polarity in a given genetic background is variable depending on the location in the wing.

Analysis of the wild-type wing revealed features of MTs with respect to alignment and asymmetry of polarity (Figures 2B, 2C, 2D, and S1D). At 14 h APF, MTs were aligned mostly along the A-P axis (see ACV and L3-1 in Figure 2B; see also Figure S1D) or in an isotropic manner (L3-3 in Figure 2B). As pupal development proceeded, the MTs converged along the P-D axis, and this P-D alignment became the most dramatic at 24 h APF at all of the 4 locations observed. Consequently, the MTs in the cells in the proximal locations rotated their directional distribution almost 90 degrees. This “P-D conversion” was transient as shown by the fact that it became partially relaxed at 30 h APF.

We also examined whether or not MT growth was asymmetrical along the P-D axis at each observation point at 24 h and found that + end-distal MTs were more abundant than + end-proximal ones in the proximal regions (green arrows in Figure 2B and double asterisks in Figure 2C; see also Figure 2D). The difference was subtle, with a 5-7% excess of + end-distal MTs, but statistically significant (see actual p-values in the legend and also Figure S2). To summarize the MT dynamics at the proximal locations of the wing (ACV and L3-1), the P-D alignment was more extreme at 24 h APF than at the other stages; and MTs grew in both proximal and distal directions, with a small excess of + ends pointing distally. To examine the subcellular distribution of microtubule organizing centers (MTOCs), we observed where in the cell the MT growth was initiated after colcemid application and subsequent inactivation by UV light (Jankovics and Brunner, 2006; Wilkie and Davis, 2001). The growth took place both at cell cortexes and in the cytoplasm (data not shown).

Both the MT alignment and the asymmetry of polarity were altered in the *ds* mutant, but neither was affected in mutants of 2 core-group genes

What are the mechanisms that underlie the above features of MT growth? We wondered whether either of the 2 groups of the PCP regulators might control the dynamics, and so we examined if the direction of growing MTs was altered in any of those mutants or not (Figures 3 and 4). As far as our analysis at 24 h APF was concerned, no significant difference was detected between the wild type and the strong loss-of-function mutants of either of these core-group genes, *fz* and *stbm*/*Vang* (Figure 3). We speculated that it would be more likely that the other group containing Ds and Ft regulated the MT growth. One reason was that Ds and Ft are proposed to play their roles in PCP before the polarized redistribution of the core proteins (Matakatsu and Blair, 2004), when the MT alignment and polarity are dynamically changing during normal development.

The *ds* or *ft* mutant wing exhibits complex phenotypes at multiple levels (Adler et al., 1998; Bryant et al., 1988; Clark et al., 1995; Garoia et al., 2000; Strutt and Strutt, 2002). At subcellular, cellular, and intercellular levels, the *ds* or *ft* mutant wing exhibited PCP phenotypes distinct from those of the core-group mutants: reverse orientation and swirling of wing hairs in the proximal region with high penetrance (compare Figures 3A and 3B with Figure 4A) and the loss of long-range coordination due to mislocalization of the core-group members and prehairs at the wrong cortical domains (Figure 4B; Ma et al., 2003; Strutt and Strutt, 2002). The genotype employed in our MT analysis was an allelic combination of *ds* (ds^{38k}/ds^{UAO71}) that persisted during pupal development with high penetrance; and we collected data at the 4 locations and at 3 ages between 18 h APF and 30 h APF, but not at 14 h APF due to a technical difficulty (Figures 4C, S1B, and S1E; see Experimental Procedures).

With regard to the alignment in the above mutant, growing MTs failed to converge along the P-D axis as strongly as in the wild type (Figures 4C, S1F, and Movies S3 and S4). This misalignment was verified by statistical analysis (Figure 4F and its legend), as suggested by the fact that the proportion of anteriorly or posteriorly oriented MTs (A-P-oriented MTs) in the mutant was larger than that in the wild-type wing. The distally biased asymmetry of MT growth in the wild type was substantially weakened in the mutant ACV and L3-1 locations at 24 h APF (Figures 4C, 4D, and 4E; see also Figure S3). Furthermore, + end-proximal MTs became more abundant at the L3-3 location where the polarity was supposed to be symmetrical (magenta arrow in Figure 4C, double asterisk in Figures 4D, and S3; see also Figure 4E). All of these results suggest that Ds was required for the normal MT alignment and asymmetry of polarity in the wing.

Bias of MT growth from high Ds to low Ds

One interesting feature of Ds is its expression pattern. It has been reported that Ds is strongly expressed in the presumptive dorsal hinge in the larval imaginal disc and in the pupal wing (Ma et al., 2003; Strutt and Strutt, 2002) and that the expression profile exhibits a proximal-high distal-low gradient during 17-26 h APF (Matakatsu and Blair, 2004). We revisited the Ds profile at 24 h APF and verified the strong expression in the hinge region (data not shown).

We suspected the possibility that this imbalance may be causative of the asymmetry of MT growth in the proximal region. To test this hypothesis, we performed the following 2 experiments: First, we made an ectopic domain of Ds expression in the most distal end of the wing (Figures 5A and 5B; Matakatsu and Blair, 2004). Second, we overrode the endogenous gradient by the high and flat exogenous expression in the posterior compartment (Figures 5C and 5D; Matakatsu and Blair, 2004).

When cells strongly positive for Ds were generated along the distal margin, wing hairs showed the reverse polarity or swirl patterns around the L3-3 location (Figure 5A; n=10). At the equivalent distal location in the control wing, MT polarity was symmetrical; in contrast, the distal ectopic Ds expression broke this symmetry and + end-proximal MTs became more abundant with no variation of anterior and posterior components (Figures 5B and 5G). These data suggest that the ectopic Ds was sufficient to bias the direction of MT growth from high Ds to low Ds. MT polarity was also reversed at the L3-3 region in the *ds* mutant wing (magenta arrow in Figure 4C), but it was not associated with the reverse hair polarity (Figure 4A). These 2 reverse MT polarity phenotypes were quantitatively different from each other, as shown by the fact that the directional distribution of MTs in the *ds* mutant was much less biased along the P-D axis and more isotropic than that in the *ds* misexpression (compare the rose diagram of L3-3 at 24 h in Figure 4C with the red one in Figure 5B; $p < 0.001$ by Pearson's χ^2 test).

Next we examined the effects of the high and flat expression of Ds in the posterior compartment on MT growth at 24 h APF (inside the red box in Figure 5C; see also Movie S5). Inside the overexpression domain, a majority of MTs aligned themselves along the P-D axis as they did in the control (Figure 5D; compare the gray and red plots of Figure 5H). Therefore the high and flat expression *per se* did not abolish the P-D alignment; in contrast, it did make the MT polarity symmetrical, as shown by the fact that MTs grew almost equally in both proximal and distal directions in the high Ds domain (Figure 5H). This result suggests that an imbalance of the Ds amount between adjacent cells was necessary for the asymmetry of MT polarity. Hair polarity was not disrupted in the posterior compartment; in contrast, the adjacent anterior cells (up to 5-6 cells) misoriented their hairs away from the anterior/posterior compartment boundary (Figure 5C; n= 12). This non-autonomous effect was consistent with the result of the ectopic *ds* expression along the distal margin (Figure 5A).

Another atypical cadherin, Ft has been proposed to be a receptor for Ds (Matakatsu and Blair, 2004, 2006; Yang et al., 2002), and so we also studied the consequences of *ft* overexpression in the posterior compartment. The overexpression caused misorientation of wing hairs inside the expression domain (Figure 5E; n=4). Under this condition, MT polarity in the proximal region was reversed with a significant excess of + end proximal MTs; and the P-D alignment of the MTs became milder (blue plots of Figures 5F and 5H; Movie S6), which was reminiscent of the *ds* mutant phenotypes.

Subcellular localization of PAR-1 in the pupal wing

How do Ds and Ft steer MT dynamics? We looked for candidate molecules that might mediate the linkage between the Ds-Ft system and the MT dynamics, and focused on the serine/threonine kinase PAR-1 (Goldstein and Macara, 2007; Suzuki and Ohno, 2006); because PAR-1 has been shown to regulate MT organization in various systems (Cox et al., 2001; Doerflinger et al., 2003; Drewes et al., 1997; Shulman et al., 2000). Based on the studies on Drosophila oocytes and follicular epithelia, PAR-1 is proposed to act primarily on plus ends to control MT polarity (Doerflinger et al., 2003). Below we report (1) a feature of the subcellular localization of PAR-1 in the wing (Figures 6 and S4), (2) that PAR-1 localization was affected at least when Ft did not function properly (Figures 7 and S5), and (3) *par-1* overexpression impaired MT dynamics and PCP, mimicking the *ds* mutant or *ft* overexpression phenotypes partially (Figure 8).

We first examined the specificity of our PAR-1 antibody in the pupal wing, and confirmed that both cortical and cytoplasmic signals did in fact represent endogenous PAR-1 molecules (Figure 6A; the number of clones observed: 10). Then we surveyed signals at distinct locations at 3 different pupal ages (Figures 6B-6E; data not shown). PAR-1 was cortically localized in most of the cells at the ages examined. After 24 h APF when the vein structures started to appear, the cortical localization became ambiguous in the veins, in contrast to that in the intervein regions (Figures 6B and 6D). Intriguingly, at 24 h APF, in restricted intervein regions around the ACV and the posterior cross vein (PCV), PAR-1 was primarily localized at anterior and posterior cortexes (A/P cortexes; Figures 6B, 6C, and S4A-S4C; number of wings observed: 11). Only within those regions, the A/P localization of PAR-1 encompassed about 10 rows of cells on each side of the cross vein. The A/P cortical localization was still observed at 30 h APF, but became less coherent than at 24 h APF (Figure 6B; n= 10). Coherent A/P localization was seen nowhere at 18 h APF (n=3). We observed MT dynamics around PCV and found that MTs were predominantly aligned along the P-D axis as they were at the ACV region (Figures S4D and S4E).

Along the apicobasal level at the cortex, it has been shown in embryos and follicular cells that PAR-1 is localized in the basolateral domain (Bayraktar et al., 2006; Shulman et al., 2000). We found that this was also the case in the wing epidermis at 24 h and 30 h APF (Figure 6F; n=6). The PAR-1 domain included those of Discs-large (Dlg) and Fasciclin III (Fas III), which are basolaterally localized (Knust and Bossinger, 2002; Woods and Bryant, 1991), and further reached the apical Fmi domain (Figure 6F; data of Dlg and Fas III are not shown). When we looked down at the plane at 24 h APF, we found that Dlg and Fas III were also localized at A/P cortexes around the cross veins, as was PAR-1 (data not shown).

The PAR-1 subcellular localization was altered when Ft did not function properly

Putting our above findings together, one naïve hypothesis would be that PAR-1 might contribute to MT dynamics governed by Ft and Ds. To test this hypothesis, we first examined whether or not the PAR-1 localization was affected when the Ds-Ft system did not function properly (Figures 7 and S5; data not shown).

We analyzed the effect of *ft* overexpression on PAR-1 localization, and found that it influenced the apicobasal localization and the level of PAR-1 (Figures 7A-7C; n=6). Upon *ft* overexpression, the cytoplasmic PAR-1 signal was strongly enhanced on the subapical plane where Ft and Ds are localized (Ma et al., 2003) and also on slightly more basal planes, possibly at the AJ where Fmi is localized (Figures 7B and 7C). Cortical signals of PAR-1 also became stronger in the overexpressing compartment than in the control anterior compartment. These changes were probably not due to altered abundance of *par-1* mRNA, as shown by our *in situ* hybridization of these pupal wings (data not shown). We also

examined PAR-1 in *ft* mutant clones. The cortical localization of PAR-1 looked obscured in *ft* mutant clones around the proximal region including the cross veins, but this result should be carefully interpreted because the layer of *ft* mutant cells exhibited morphological defects (Figures S5A, S5B, S5D, and S5E; see also Bryant et al., 1988).

In mammalian epithelial cells and Xenopus embryo, the atypical protein kinase C (aPKC) regulates plasma membrane localization of PAR-1 (Hurov et al., 2004; Kusakabe and Nishida, 2004; Suzuki et al., 2004). Furthermore, it has been recently reported that the amount of apical complexes, including aPKC, is increased in imaginal disc cells when the hippo-signaling pathway in which Ft functions as a receptor is impaired and that this increase is dependent on the transcriptional regulator Yorkie (Hamaratoglu et al., 2009). With these previous studies in mind, we stained pupal wings for aPKC. The aPKC level was increased in *ft* clones in the pupal wing (Figures S5C and S5F), as expected from the study in the disc; and conversely, it was decreased in the *ft* over-expression domain (Figures 7D and 7E). Thus it appears that the mislocalization of PAR-1 by *ft* over-expression was mediated by a decrease in the aPKC level. In addition to PAR-1 and aPKC, we examined the signal intensity of Fmi at the AJ, and found that it was substantially reduced; although the cell-border signal was still detected (Figures 7A, 7C, and 7E). We further addressed whether or not the mislocalization and/or up-regulation of PAR-1 contributed to the *ft*-overexpression (*ft*+) PCP phenotype (Figures 5E and 7F-7H). This seemed likely as suggested by the fact that the *ft*+ hair-polarity phenotype was significantly suppressed when *par-1* was knocked down in the same posterior compartment (Figures 7I-7L). In contrast to the studies on *ft*, we did not see obvious effect on the PAR-1 localization in *ds* clones and *ds*-overexpressing wings (data not shown).

par-1 overexpression phenocopied the *ds* mutant or *ft* overexpression phenotypes of PCP and MT dynamics

Next we addressed whether PAR-1 was relevant to the MT dynamics and PCP in the wing or not (Figures 8, S6, and Movie S7). When *par-1* was overexpressed widely by using the *c765-GAL4* driver, wing hairs were misoriented primarily in a proximal region up to the L3-1 location, but the hair-polarity defect was not seen beyond it (Figure 8A; n=22). In this proximal region, subpopulations of P-D-oriented MTs were decreased with a concomitant increase in those of A-P-oriented ones; and in addition, the P-D asymmetry of MT polarity became milder and no longer statistically significant (Figures 8B-8D). With respect to Fmi localization, the coherent zigzag pattern at P/D cell boundaries was disorganized, and Fmi was present ectopically at A/P cell boundaries (Figures 8E and 8F; see arrows in Figure 8F; n=5). Furthermore, wing hairs were generated at cell vertexes that were connected to those Fmi-mislocalized A/P boundaries (Figure 8F). As far as this proximal region was concerned, all of these phenotypes were reminiscent of those of the *ds* mutant (Figure 4) or *ft* overexpression (Figure 5E). Expression of a kinase-inactive form of PAR-1 did not cause any visible abnormality, showing that all of the above phenotypes were dependent on PAR-1 kinase activity (data not shown). Collectively, our data support the possibility that the MT dynamics during normal development is relevant to PCP, and suggest that at least Ft controls the MT dynamics by way of regulating the subcellular localization and/or the activity of PAR-1 in the proximal region.

Although it has been shown that overexpression of PAR-1 disrupts apicobasal cell organization in the eye disc (Bayraktar et al., 2006), our *c765*-driven expression did not cause an obvious defect in the apicobasal polarity (Figures 8G and 8H; n=7). We also examined how the loss of or reduction in *par-1* function affected MT and PCP, and found pleiotropic defects including abnormal MT growth and subtle mis-orientation of wing hairs (Figure S6; see details in the legend).

Discussion

Ds and Ft-dependent control of the MT growth was required for normal PCP in the proximal region

We revealed 2 features of the dynamics of planar noncentrosomal MTs in the wild-type wing cells with respect to alignment and asymmetry of polarity, and this was dependent on the Ds-Ft system. In the *ds* mutant, MTs still aligned along the axis, albeit to a lesser degree. This may be due to the fact the *ds* mutant wing includes cells with relatively normal polarity (Adler et al., 1998; see L3-1 in Figure 4A) and/or the possibility that substantial activity of Ft remains even in the absence of Ds (Matakatsu and Blair, 2004, 2006) and Ft alone could partially contribute to the MT alignment. About the asymmetry of MT polarity, our data verified the hypothesis that the imbalance of the Ds level directs MT growth from high Ds to low Ds, which is consistent with the idea that the direction of Ds gradient determines the direction of cell polarity (Rogulja et al., 2008; Willecke et al., 2008).

It is likely that the MT dynamics described above is relevant to PCP. This conclusion is based on the consequences of the perturbation of the MT dynamics by the *par-1* overexpression, in which the individual cells were polarized but were not coordinated with the P-D axis, being reminiscent of the *ds* mutant or *ft* overexpression phenotype. It should be emphasized that this overexpression effect provided a striking contrast to those effects caused by application of MT drugs or by overexpressing a MT-depolymerizing kinesin (Shimada et al., 2006). Such destructive treatments result in severe phenotypes, some of which are reminiscent of those of core-group mutants (loss of core members at cell boundaries and formation of wing hairs at apical cell centers). All these data support the idea that the steering of MT growth is required for adjusting the individual cell polarity along the P-D axis, leading to the long-range coordination.

The results of previous rescue experiments on the *ds* or *ft* mutants may be explained in the above context. Each mutant PCP phenotype is recovered to normal by uniform expression of *ds* or *ft*, except for a limited region proximal to the ACV (Matakatsu and Blair, 2004, 2006). This region-specific failure could be due to the absence of a sufficient imbalance of the Ds level.

In the wild type, the significant asymmetry of MT growth was restricted up to L3-1~L3-2 at the farthest, and asymmetry was not detected in more distal regions. Yet distally-oriented hair polarity was robust throughout the wing. The coordination of the axis and the single cell polarity in the distal region may be dependent on the input to Ft through phosphorylation by Four-jointed that is expressed high in the distal (Brittle et al., 2010; Ishikawa et al., 2008; Simon et al., 2010). Another possibility is that local cell-cell communication, which is mediated by the core-group proteins, may play pivotal roles in the coordination (Chen et al., 2008; Strutt and Strutt, 2008, 2009; Wu and Mlodzik, 2008). In fact, the Ds-Ft pathway and the PCP core group are proposed to act in either a semi-independent or a parallel fashion in some contexts of PCP (Axelrod, 2009; Lawrence et al., 2007; Strutt, 2008; Wu and Mlodzik, 2009).

A hypothetical connection between the Ds-Ft system, PAR-1, and MTs

Two previous studies have provided leads about a connection between the Ds-Ft system and MTs in mitotic spindles: Oriented cell divisions (OCD) are defective in the imaginal discs of *ds* or *ft* mutants and also in kidney development in *fat4* knock-out mice (Baena-López et al., 2005; Saburi et al., 2008). However, little is known about the molecular mechanisms involved.

As a candidate molecule that serves as a mediator between the Ds-Ft system and the MT dynamics in the pupal wing, we focused on PAR-1, whose subcellular localization was affected at least by Ft by way of altering aPKC. We would like to point out that a substantial amount of PAR-1 was detected in the cytoplasm in the wild type cells and that the levels of both cytoplasmic and cortical PAR-1 signals were elevated by *ft* overexpression. These data indicate the possibility that cytoplasmic pool of PAR-1 may also contribute to the MT organization.

One feature of PAR-1 was its A/P cortical localization, which spatiotemporally coincided with the strong P-D alignment of the MTs around the cross vein regions. It has been demonstrated that *ft* mutant clones only around these regions show significant polarity defects (Strutt and Strutt, 2002). In addition, it has been proposed that the Ft is necessary for the propagation of polarity signals across a field of cells with irregular cell shapes, including the cross veins (Ma et al., 2008). The PAR-1 at A/P cell boundaries and/or strong MT alignment might play a pivotal role in the function of Ft to propagate PCP signals across the cross veins regions. In light of the mechanism of PAR-1 that have been proposed to be at work in Drosophila follicular epithelium and oocytes, PAR-1 at the A/P cortexes may contribute to the convergence of growing MTs by capping MT + ends, thereby preventing them from growth (Doerflinger et al., 2003).

The PAR-1 data presented in this study may not explain all aspects of the MT dynamics we observed. For example, the localization of PAR-1 was polarized in the very restricted regions, whereas the alignment of the MTs was observed throughout the wing at 24 h APF, despite the fact that the degree of convergence was weaker towards the distal end of the wing. Another unsolved question is the origin of the asymmetry of MT polarity. Although MT asymmetry was abrogated either by loss-of-function or overexpression of PAR-1, the localization and the level of PAR-1 was obviously affected neither in *ds* mutant clones nor around *ds*-overexpressing domains. Our data indicate that the expression pattern of Ds plays an instructive role in generating the asymmetry of MT polarity. These results raise the possibility that there may exist other players to decode instructional information of the Ds expression and control MTs. It has been reported that *widerborst* (*wdb*) that encodes the B′ regulatory subunit of protein phosphatase 2A (PP2A) plays roles in cortical polarization and MT organization in the Drosophila wing. Interestingly, Wdb is enriched on distal MT bundles within pupal wing cells before hair formation (Hannus et al., 2002). PP2A antagonizes the kinase activity of PAR-1 in several developmental contexts (Kao et al., 2004; Krahn et al., 2009; Nam et al., 2007; Yoder et al., 2004), so we speculate the possibility that PP2A and PAR-1 may control MT polarity by way of unknown substrates, which regulate MT organization.

MTs, cell geometry, and planar polarity

ds or *ft* viable mutations cause multiple phenotypes in the wing, including foreshortening along the P-D axis, the PCP phenotypes, and changes in cell geometry (Adler et al., 1998; Bryant et al., 1988; Clark et al., 1995; Garoia et al., 2000; Ma et al., 2003, 2008; Strutt and Strutt, 2002). At a first glance, the proximal ACV and L3-1 locations in the *ds* mutant included cells that looked less stretched along the P-D axis (T. H. and T. U., unpublished data). Considering that there is a feedback between MT organization and cell geometry (Hamant et al., 2008), it might be difficult to clarify the cause-and-effect relationship between the phenotypes of MT dynamics and “fat” cells with shorter P-D boundaries in *ds* mutants. Nonetheless the L3-3 cells, in which MT polarity was reversed by the ectopic *ds* expression, appeared to be normal in the shape (data not shown), suggesting the possibility that Ds and Ft at the subapical domain may control the apical MTs, through a machinery separate from the cell geometry.

The role of the MT dynamics: How does it contribute to asymmetric localization of Fz?

Coming back to the role of the MT-dependent polarized transport of Fz-containing vesicles that we have proposed (Shimada et al., 2006), how does it contribute to PCP? One possibility is that the directional transport plays a pivotal role in setting up a small bias of Fz activity across the P/D cell boundary, which is subsequently amplified by a positive feedback loop (Axelrod, 2009). Another non-mutually exclusive possibility is that the transport is critical for Fz to recycle back to the distal membrane domain, tethering a sufficient number of Fz molecules there together with Fmi to achieve the asymmetric localization (Strutt and Strutt, 2009). In either possibility, how can such a small difference in the MT polarity be causally related to the distally oriented transport? Quantitative imaging of *oskar* mRNA transport in the living Drosophila oocytes has demonstrated that the mRNA becomes localized at the posterior pole by a biased random walk along weakly polarized A-P MTs (Zimyanin et al., 2008). Having analyzed the dynamics of planar MTs, we are now tracking Fz vesicles and exploring statistical properties of their movements in the pupal wing epidermis (T. J. K., T. H., H. R. U., and T. U., unpublished data). Once we find the rules that govern the transport in the wild type, it would be important to track the vesicles under the condition of the reverse MT polarity and address how the transport is affected, thereby providing mechanistic insights into the directional transport in the context of PCP.

Experimental procedures

Time-lapse observation of living pupal wing cells

Details of mounting pupae were essentially as described in the legend of Supplemental Figure S1B of Shimada et al. (2006). Briefly, each pupa was placed on double-sticky scotch tape, and a small piece of the pupal case over a wing was peeled off with forceps. After moistening the glue by adding water, each pupa was removed from the tape and put on a 35-mm glass-bottomed dish (IWAKI) with the peeled side down. Each pupa was slightly tilted by using a drop of grease (Dow Corning Toray) as a “pillow” to attach the peeled area to the glass and make observation of the epidermal plane easy. The pupae were supported by wet filter paper, which was also helpful to prevent desiccation. The dish was sealed with PARAFILM.

Movies of EB1-GFP signals in dorsal wing epidermis were acquired by using a spinning-disk confocal scan head (CSU10; Yokogawa) that was mounted on an Olympus IX71 microscope (60× water-immersion objective) equipped with an EM-CCD camera (DU-888; Andor Technology). Fluorescent proteins were excited with a 488 nm line for GFP and a 561 nm line for mRFP and mCherry from diode-pumped solid-state lasers (Coherent and Cobolt, respectively), and detected with a 500-550 nm and 580-640 nm band-pass filter, respectively. The exposure time was 500 ms for 488 nm and 100 ms for 561 nm, and the EM gain of the camera was 1000×. The output of the 488 nm laser power and that of the 561 nm one were 30% (approx. 0.2 mW) and 100% (approx. 0.3 mW), respectively. Typically, single confocal planes were taken at 1-sec intervals for our image collection of EB1-GFP only and at 2-sec intervals for the two-color imaging, for a total of 10 frames. The above hardware was driven by MetaMorph (Molecular Device). After the imaging, we kept those pupae at 25 °C and confirmed that they survived to at least the pharate stage. Some of 14 h APF pupae did not give EB1-GFP signals, possibly because they were appeared to be sensitive to the damage, and became unhealthy once small pieces of the pupal cases had been peeled off. This happened in the case of the wild type and more frequently in that of the *ds* mutant. Those pupae negative for EB1-GFP signals did not develop and that was why we did not collect data on the *ds* mutant.

Quantification and statistical analysis

EB1-GFP comets were abundant in the apical MT web at the level of the adherens junction (Shimada et al., 2006). To collect data on the directions of MT growth, we tracked those comets by using the measurement tool ”Region Measurements” of MetaMorph (Molecular Device). The angle of each comet was calibrated in reference to the P-D axis of the wing that was defined as a line connecting locations of the 3 sensory organs on the L3 vein (L3-1, L3-2, and L3-3 in Figures S1A and S1B). At each spatiotemporal point for a given genotype, 1,000~2,000 comets were tracked from over 10-20 animals. The directional distribution of EB1-GFP comets was evaluated with and shown as Rose diagrams (Rose 2.1.0). The Rose diagrams show the frequency of EB1-GFP directions in the cells directed into 18 bins of 20°, representing 360° around the starting point of each EB1-GFP track. Rose 2.1.0 was obtained from the Todd A. Thompson's Web Site (http://mypage.iu.edu/~tthomps/programs/home.htm).

To evaluate the directional preference of comet movements, we sorted original data sets of the direction into 4 sectors of 90° each (Figure 1I). Then we compared values of the distal sectors (-45°~45°; green in Figures 1I and 1J) with those of the proximal ones (135°~225°; magenta in Figures 1I and 1J) by the Wilcoxon signed-rank test to address which were more abundant, + end-distal MTs or + end-proximal ones. The percentage of each direction was presented as dot plots (Figure 1J). We also compared the frequency of + ends in each direction between different genotypes by using the Pearson's χ^2 test. The percentage of each direction was presented as bar plots (Figures 4F, 8D, and S6D). R version 2.9.2 (The R Foundation for Statistical Computing) was used for both tests.

Supplementary Material

Refer to Web version on PubMed Central for supplementary material.

Acknowledgments

DGRC at Kyoto Institute of Technology, the Bloomington Stock Center, the NIG stock center and the Developmental Studies Hybridoma Bank at the University of Iowa provided fly stocks and the antibodies. We thank S. Yonemura, M. Takeichi, S. Hayashi, and members of Yonemura's lab for allowing T.H. and Y.S. to perform EM studies in CDB, RIKEN. We are also grateful to D. Strutt, K. Irvine, H. Matakatsu, S. Blair, H. Ohkura, D. Woods, and S. Hayashi for providing other fly strains and reagents. We thank very much T. Fujimori for his critical technical advice; members of Uemura's lab for discussion; and Y. Miyake, K. Shimizu and M. Futamata for their technical assistance. This work was supported by a CREST grant to T.U. from JST and by NIH grants R01 NS043167, R01 AR054926, and R01 MH080378 to B.L. Y.S. was a recipient of a Fellowship of the Japan Society for the Promotion of Science for Junior Scientists. T.J.K. was supported by a Grant-in-Aid for Scientific Research on Innovative Areas (21116006).

References

Adler PN, Charlton J, Liu J. Mutations in the cadherin superfamily member gene dachsous cause a tissue polarity phenotype by altering frizzled signaling. Development. 1998; 125:959–968. [PubMed: 9449678]

Adler PN. Planar signaling and morphogenesis in Drosophila. Dev Cell. 2002; 2:525–535. [PubMed: 12015961]

Axelrod JD. Progress and challenges in understanding planar cell polarity signaling. Semin Cell Dev Biol. 2009; 20:964–971. [PubMed: 19665570]

Baena-López LA, Baonza A, García-Bellido A. The orientation of cell divisions determines the shape of Drosophila organs. Curr Biol. 2005; 15:1640–1644. [PubMed: 16169485]

Bayraktar J, Zygmunt D, Carthew RW. Par-1 kinase establishes cell polarity and functions in Notch signaling in the Drosophila embryo. J Cell Sci. 2006; 119:711–721. [PubMed: 16449319]

Brittle AL, Repiso A, Casal J, Lawrence PA, Strutt D. Four-Jointed Modulates Growth and Planar Polarity by Reducing the Affinity of Dachsous for Fat. Curr Biol. 2010; 20:803–810. [PubMed: 20434337]

Bryant PJ, Huettner B, Held LI, Ryerse J, Szidonya J. Mutations at the fat locus interfere with cell proliferation control and epithelial morphogenesis in Drosophila. Dev Biol. 1988; 129:541–554. [PubMed: 3417051]

Chae J, Kim MJ, Goo JH, Collier S, Gubb D, Charlton J, Adler PN, Park WJ. The Drosophila tissue polarity gene starry night encodes a member of the protocadherin family. Development. 1999; 126:5421–5429. [PubMed: 10556066]

Chen W, Antic D, Matis M, Logan CY, Povelones M, Anderson GA, Nusse R, Axelrod JD. Asymmetric homotypic interactions of the atypical cadherin flamingo mediate intercellular polarity signaling. Cell. 2008; 133:1093–1105. [PubMed: 18555784]

Clark HF, Brentrup D, Schneitz K, Bieber A, Goodman C, Noll M. Dachsous encodes a member of the cadherin superfamily that controls imaginal disc morphogenesis in Drosophila. Genes Dev. 1995; 9:1530–1542. [PubMed: 7601355]

Classen A, Anderson KI, Marois E, Eaton S. Hexagonal packing of Drosophila wing epithelial cells by the planar cell polarity pathway. Dev Cell. 2005; 9:805–817. [PubMed: 16326392]

Cox DN, Lu B, Sun TQ, Williams LT, Jan YN. Drosophila par-1 is required for oocyte differentiation and microtubule organization. Curr Biol. 2001; 11:75–87. [PubMed: 11231123]

Doerflinger H, Benton R, Shulman JM, St Johnston D. The role of PAR-1 in regulating the polarised microtubule cytoskeleton in the Drosophila follicular epithelium. Development. 2003; 130:3965–3975. [PubMed: 12874119]

Drewes G, Ebneth A, Preuss U, Mandelkow EM, Mandelkow E. MARK, a novel family of protein kinases that phosphorylate microtubule-associated proteins and trigger microtubule disruption. Cell. 1997; 89:297–308. [PubMed: 9108484]

Eaton S, Wepf R, Simons K. Roles for Rac1 and Cdc42 in planar polarization and hair outgrowth in the wing of Drosophila. J Cell Biol. 1996; 135:1277–1289. [PubMed: 8947551]

Eaton S. Cell biology of planar polarity transmission in the Drosophila wing. Mech Dev. 2003; 120:1257–1264. [PubMed: 14623436]

Feng Y, Irvine KD. Processing and phosphorylation of the Fat receptor. Proc Natl Acad Sci USA. 2009; 106:11989–11994. [PubMed: 19574458]

Fristrom D, Fristrom JW. The mechanism of evagination of imaginal discs of Drosophila melanogaster. 1. General considerations. Dev Biol. 1975; 43:1–23. [PubMed: 807489]

Garoia F, Guerra D, Pezzoli MC, López-Varea A, Cavicchi S, García-Bellido A. Cell behaviour of Drosophila fat cadherin mutations in wing development. Mech Dev. 2000; 94:95–109. [PubMed: 10842062]

Goldstein B, Macara IG. The PAR proteins: fundamental players in animal cell polarization. Dev Cell. 2007; 13:609–622. [PubMed: 17981131]

Hamant O, Heisler MG, Jönsson H, Krupinski P, Uyttewaal M, Bokov P, Corson F, Sahlin P, Boudaoud A, Meyerowitz EM, et al. Developmental patterning by mechanical signals in Arabidopsis. Science. 2008; 322:1650–1655. [PubMed: 19074340]

Hamaratoglu F, Gajewski K, Sansores-Garcia L, Morrison C, Tao C, Halder G. The Hippo tumor-suppressor pathway regulates apical-domain size in parallel to tissue growth. J Cell Sci. 2009; 122:2351–2359. [PubMed: 19531584]

Hannus M, Feiguin F, Heisenberg C, Eaton S. Planar cell polarization requires Widerborst, a B′ regulatory subunit of protein phosphatase 2A. Development. 2002; 129:3493–3503. [PubMed: 12091318]

Hurov JB, Watkins JL, Piwnica-Worms H. Atypical PKC phosphorylates PAR-1 kinases to regulate localization and activity. Curr Biol. 2004; 14:736–741. [PubMed: 15084291]

Ishikawa HO, Takeuchi H, Haltiwanger RS, Irvine KD. Four-jointed is a Golgi kinase that phosphorylates a subset of cadherin domains. Science. 2008; 321:401–404. [PubMed: 18635802]

Jankovics F, Brunner D. Transiently reorganized microtubules are essential for zippering during dorsal closure in Drosophila melanogaster. Dev Cell. 2006; 11:375–385. [PubMed: 16908221]

Kao G, Tuck S, Baillie D, Sundaram MV. C. elegans SUR-6/PR55 cooperates with LET-92/protein phosphatase 2A and promotes Raf activity independently of inhibitory Akt phosphorylation sites. Development. 2004; 131:755–765. [PubMed: 14724126]

Knust E, Bossinger O. Composition and formation of intercellular junctions in epithelial cells. Science. 2002; 298:1955–1959. [PubMed: 12471248]

Krahn MP, Egger-Adam D, Wodarz A. PP2A antagonizes phosphorylation of Bazooka by PAR-1 to control apical-basal polarity in dividing embryonic neuroblasts. Dev Cell. 2009; 16:901–908. [PubMed: 19531360]

Kusakabe M, Nishida E. The polarity-inducing kinase Par-1 controls Xenopus gastrulation in cooperation with 14-3-3 and aPKC. EMBO J. 2004; 23:4190–4201. [PubMed: 15343271]

Lawrence PA, Struhl G, Casal J. Planar cell polarity: one or two pathways? Nat Rev Genet. 2007; 8:555–563. [PubMed: 17563758]

Lawrence PA. Gradients in the Insect Segment: The Orientation of Hairs in the Milkweed Bug Oncopeltus Fasciatus. J Exp Biol. 1966; 44:607–620.

Ma D, Amonlirdviman K, Raffard RL, Abate A, Tomlin CJ, Axelrod JD. Cell packing influences planar cell polarity signaling. Proc Natl Acad Sci USA. 2008; 105:18800–18805. [PubMed: 19022903]

Ma D, Yang C, McNeill H, Simon MA, Axelrod JD. Fidelity in planar cell polarity signalling. Nature. 2003; 421:543–547. [PubMed: 12540853]

Matakatsu H, Blair SS. Interactions between Fat and Dachsous and the regulation of planar cell polarity in the Drosophila wing. Development. 2004; 131:3785–3794. [PubMed: 15240556]

Matakatsu H, Blair SS. Separating the adhesive and signaling functions of the Fat and Dachsous protocadherins. Development. 2006; 133:2315–2324. [PubMed: 16687445]

Nam S, Mukhopadhyay B, Choi K. Antagonistic functions of Par-1 kinase and protein phosphatase 2A are required for localization of Bazooka and photoreceptor morphogenesis in Drosophila. Dev Biol. 2007; 306:624–635. [PubMed: 17475233]

Rogulja D, Rauskolb C, Irvine KD. Morphogen control of wing growth through the Fat signaling pathway. Dev Cell. 2008; 15:309–321. [PubMed: 18694569]

Saburi S, Hester I, Fischer E, Pontoglio M, Eremina V, Gessler M, Quaggin SE, Harrison R, Mount R, McNeill H. Loss of Fat4 disrupts PCP signaling and oriented cell division and leads to cystic kidney disease. Nat Genet. 2008; 40:1010–1015. [PubMed: 18604206]

Shimada Y, Yonemura S, Ohkura H, Strutt D, Uemura T. Polarized transport of Frizzled along the planar microtubule arrays in Drosophila wing epithelium. Dev Cell. 2006; 10:209–222. [PubMed: 16459300]

Shindo A, Yamamoto TS, Ueno N. Coordination of cell polarity during Xenopus gastrulation. PLoS ONE. 2008; 3:e1600. [PubMed: 18270587]

Shulman JM, Benton R, St Johnston D. The Drosophila homolog of C. elegans PAR-1 organizes the oocyte cytoskeleton and directs oskar mRNA localization to the posterior pole. Cell. 2000; 101:377–388. [PubMed: 10830165]

Simon MA. Planar cell polarity in the Drosophila eye is directed by graded Four-jointed and Dachsous expression. Development. 2004; 131:6175–6184. [PubMed: 15548581]

Simon MA, Xu A, Ishikawa HO, Irvine KD. Modulation of Fat:Dachsous Binding by the Cadherin Domain Kinase Four-Jointed. Curr Biol. 2010; 20:811–817. [PubMed: 20434335]

Sopko R, Silva E, Clayton L, Gardano L, Barrios-Rodiles M, Wrana J, Varelas X, Arbouzova NI, Shaw S, Saburi S, et al. Phosphorylation of the tumor suppressor fat is regulated by its ligand Dachsous and the kinase discs overgrown. Curr Biol. 2009; 19:1112–1117. [PubMed: 19540118]

Strutt DI. Asymmetric localization of frizzled and the establishment of cell polarity in the Drosophila wing. Mol Cell. 2001; 7:367–375. [PubMed: 11239465]

Strutt D. The planar polarity pathway. Curr Biol. 2008; 18:R898–902. [PubMed: 18957230]

Strutt H, Strutt D. Asymmetric localisation of planar polarity proteins: Mechanisms and consequences. Semin Cell Dev Biol. 2009; 20:957–963. [PubMed: 19751618]

Strutt H, Strutt D. Differential stability of flamingo protein complexes underlies the establishment of planar polarity. Curr Biol. 2008; 18:1555–1564. [PubMed: 18804371]

Strutt H, Strutt D. Nonautonomous planar polarity patterning in Drosophila: dishevelled-independent functions of frizzled. Dev Cell. 2002; 3:851–863. [PubMed: 12479810]

Suzuki A, Hirata M, Kamimura K, Maniwa R, Yamanaka T, Mizuno K, Kishikawa M, Hirose H, Amano Y, Izumi N, et al. aPKC acts upstream of PAR-1b in both the establishment and maintenance of mammalian epithelial polarity. Curr Biol. 2004; 14:1425–1435. [PubMed: 15324659]

Suzuki A, Ohno S. The PAR-aPKC system: lessons in polarity. J Cell Sci. 2006; 119:979–987. [PubMed: 16525119]

Tree DRP, Shulman JM, Rousset R, Scott MP, Gubb D, Axelrod JD. Prickle mediates feedback amplification to generate asymmetric planar cell polarity signaling. Cell. 2002; 109:371–381. [PubMed: 12015986]

Turner CM, Adler PN. Distinct roles for the actin and microtubule cytoskeletons in the morphogenesis of epidermal hairs during wing development in Drosophila. Mech Dev. 1998; 70:181–192. [PubMed: 9510034]

Usui T, Shima Y, Shimada Y, Hirano S, Burgess RW, Schwarz TL, Takeichi M, Uemura T. Flamingo, a seven-pass transmembrane cadherin, regulates planar cell polarity under the control of Frizzled. Cell. 1999; 98:585–595. [PubMed: 10490098]

Vinson CR, Conover S, Adler PN. A Drosophila tissue polarity locus encodes a protein containing seven potential transmembrane domains. Nature. 1989; 338:263–264. [PubMed: 2493583]

Wang Y, Nathans J. Tissue/planar cell polarity in vertebrates: new insights and new questions. Development. 2007; 134:647–658. [PubMed: 17259302]

Wilkie GS, Davis I. Drosophila wingless and pair-rule transcripts localize apically by dynein-mediated transport of RNA particles. Cell. 2001; 105:209–219. [PubMed: 11336671]

Willecke M, Hamaratoglu F, Sansores-Garcia L, Tao C, Halder G. Boundaries of Dachsous Cadherin activity modulate the Hippo signaling pathway to induce cell proliferation. Proc Natl Acad Sci USA. 2008; 105:14897–14902. [PubMed: 18809931]

Woods DF, Bryant PJ. The discs-large tumor suppressor gene of Drosophila encodes a guanylate kinase homolog localized at septate junctions. Cell. 1991; 66:451–464. [PubMed: 1651169]

Wu J, Mlodzik M. A quest for the mechanism regulating global planar cell polarity of tissues. Trends Cell Biol. 2009; 19:295–305. [PubMed: 19560358]

Wu J, Mlodzik M. The frizzled extracellular domain is a ligand for Van Gogh/Stbm during nonautonomous planar cell polarity signaling. Dev Cell. 2008; 15:462–469. [PubMed: 18804440]

Yang C, Axelrod JD, Simon MA. Regulation of Frizzled by fat-like cadherins during planar polarity signaling in the Drosophila compound eye. Cell. 2002; 108:675–688. [PubMed: 11893338]

Yoder JH, Chong H, Guan K, Han M. Modulation of KSR activity in Caenorhabditis elegans by Zn ions, PAR-1 kinase and PP2A phosphatase. EMBO J. 2004; 23:111–119. [PubMed: 14685271]

Zallen JA. Planar polarity and tissue morphogenesis. Cell. 2007; 129:1051–1063. [PubMed: 17574020]

Zimyanin VL, Belaya K, Pecreaux J, Gilchrist MJ, Clark A, Davis I, St Johnston D. In vivo imaging of oskar mRNA transport reveals the mechanism of posterior localization. Cell. 2008; 134:843–853. [PubMed: 18775316]

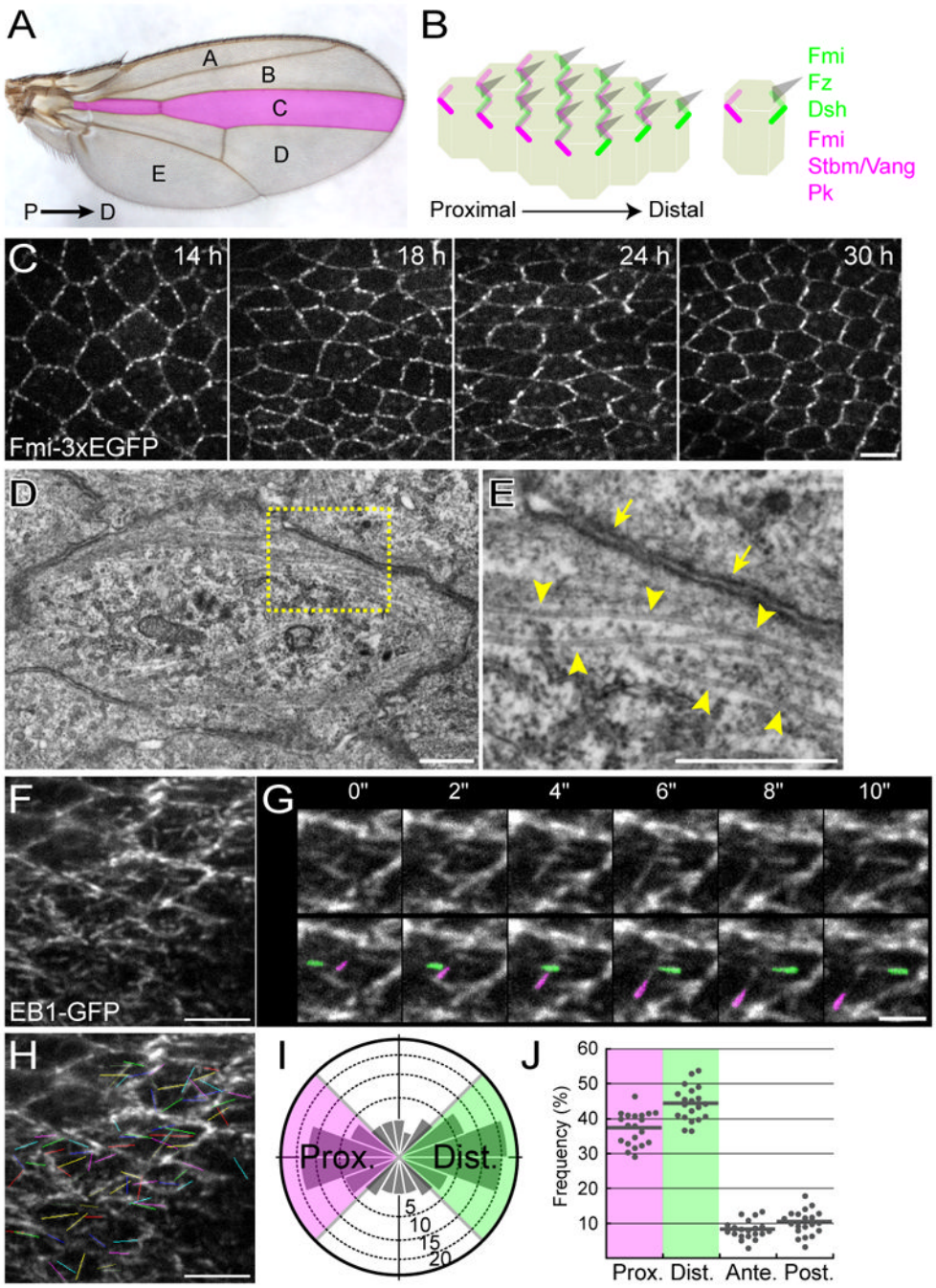

Figure 1. Subcellular localization of core members, P-D oriented MTs, and tracking growing ends of the MTs

(A) Dorsal view of the adult wing. In this and all subsequent figures, distal is to the right and anterior is at the top. Indicated are regions A-E, which are demarcated by veins and wing margins. The region C, which was mostly observed in this study, is colored in magenta.

(B) Diagrams of pupal wing epidermal cells just after the onset of prehair formation at 30-33 h after puparium formation (APF). Fmi: Flamingo; Fz: Frizzled; Dsh: Dishevelled; Stbm/Vang: Strabismus/Van Gogh; and Pk: Prickle. All of the wing hairs (gray wedges) are generated at distal cell vertexes and point distally.

(C) Time-line and temporal dynamics of Fmi-3×EGFP localization around L3-1 in the region C. The “zigzag” pattern of Fmi is most coherent at 30 h APF, just prior to the onset of hair formation. All of the relevant genotypes in this and subsequent figures are described in Supplements.

(D and E) EM images of a plane at the level of the adherens junction (AJ) at 24 h APF. A high-power image of the boxed area is shown in “E.” (E) Electron-dense domains (yellow arrows) correspond to the AJ, and arrowheads indicate P-D-oriented microtubules (MTs).

(F and G) L3-1 location (see Figure 2A) in the dorsal wing epidermis that expressed EB1-GFP (F) and images of consecutive time points at 2-sec intervals (G) at 24 h APF. In “G,” the top images were duplicated in the bottom ones, and examples of the EB1-GFP comets were painted green and magenta in the latter.

(H-J) Tracking EB1-GFP comets and statistical analysis. Movements of the comets in “F” were tracked (H), and the directional distribution of the comets is shown as a rose diagram composed of 18 bins of 20° each (I). The area of each bin represents the comets in that bin as a percentage of the total population of the comets tracked, and concentric circles are drawn with 5% increments between them. When we examined the directional preference, we compared values of the distal quadrants (-45°~45°; green in I and J) with those of the proximal ones (135°~225°; magenta in I and J). Each datum dot corresponds to the percentage of comets in each quadrant at a single observation point, and short horizontal bars are the means. Bar scales: 5 μm (C, F, and H), 500 nm (D and E), and 2 μm (G).

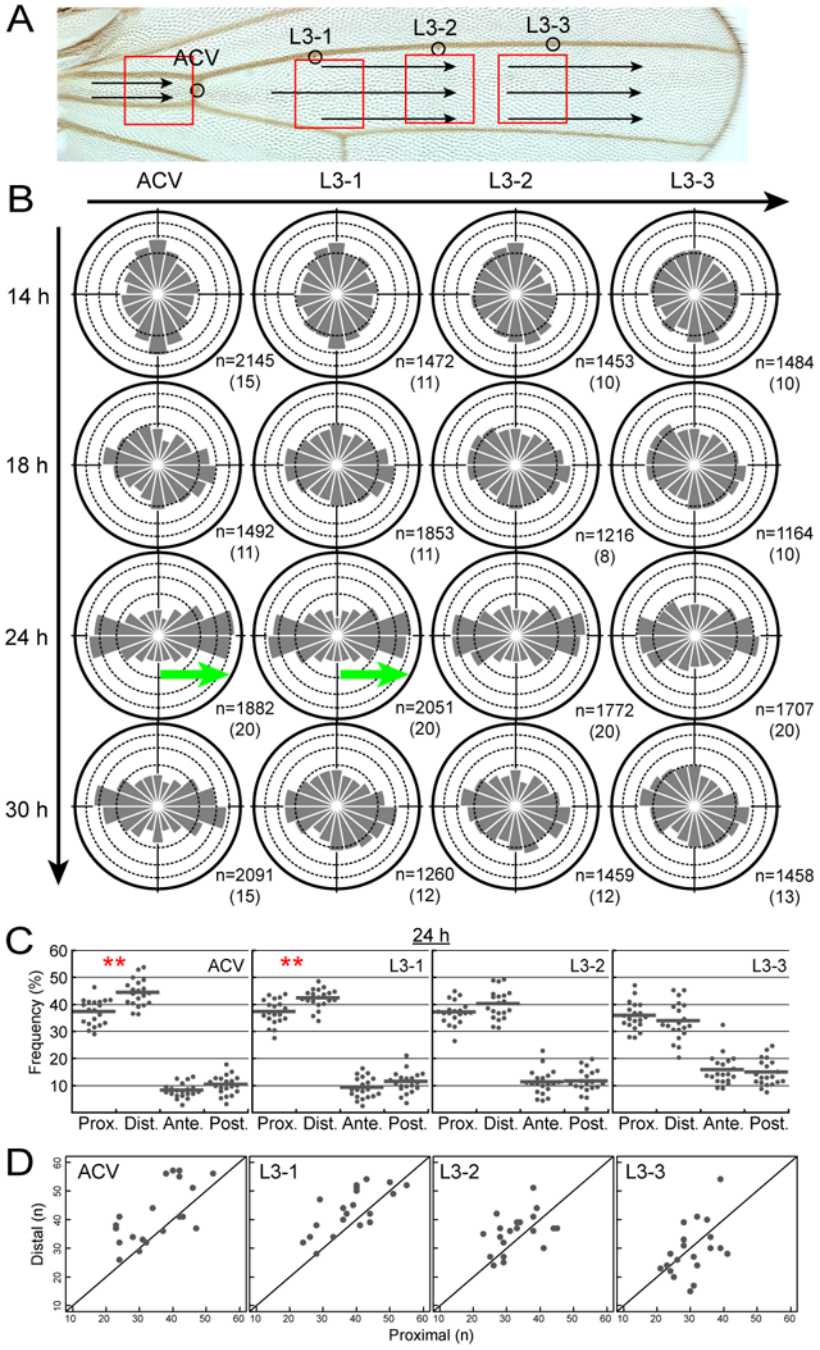

Figure 2. Spatiotemporal dynamics of MTs in the wild-type wing

(A) Indicated by red boxes are 4 distinct locations in the wild-type wing where MT growth was observed. The image of the adult wing was used for clarity (see images of pupal wings in Figure S1A). 4 campaniform sensilla were used as spatial landmarks (circles). Arrows represent the polarity of wing hairs on the dorsal surface.

(B) The directional distribution of MT growth. The horizontal axis on the top represents the P-D position; and the vertical on the left, the pupal age. Green arrows indicate statistically significant asymmetry of MT polarity with an excess of + end-distal MTs at 24 h APF. Indicated at the lower right-hand corner of each diagram is the number of EB1-GFP comets tracked and that of the wing from which the data were collected (in parentheses).

(C) Statistical analysis of the directional preference of the EB1-GFP comets at 24 h APF. + end-distal MTs were more abundant than + end-proximal ones at the ACV and L3-1 locations [**: $p < 0.01$; Wilcoxon signed-rank test; actual p-values were 0.003724 (ACV) and 0.004227 (L3-1)].

(D) The number of proximally shooting comets and that of distally shooting ones in each sample at each location at 24 h APF were plotted on X and Y axes, respectively, together with a 45 degree line.

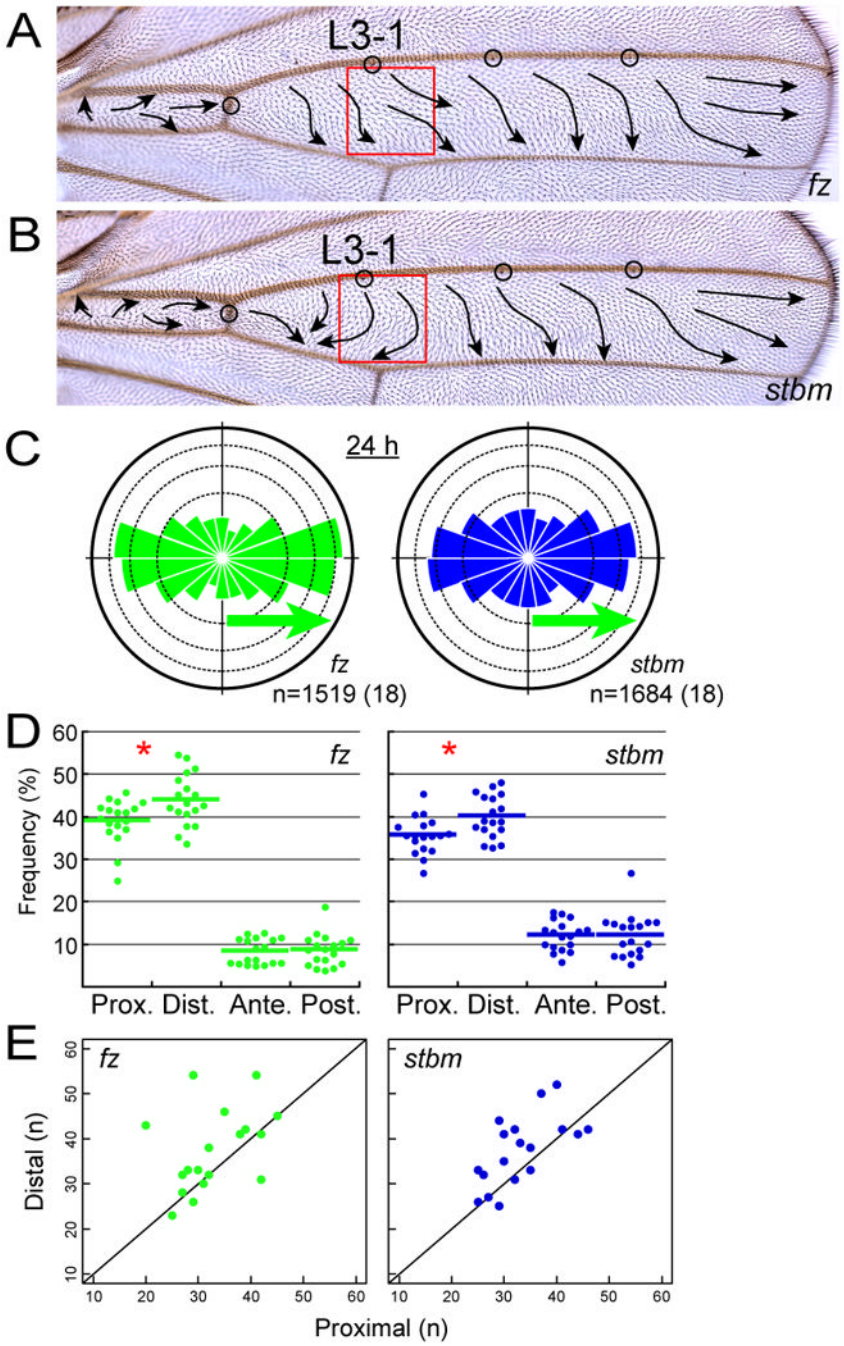

Figure 3. The directional preference of growing MTs in *fz* and *stbm* mutant wing cells

(A and B) Adult wings of *fz* (A) and *stbm* (B) mutants. Arrows represent the polarity of wing hairs on the dorsal surface. Red boxes indicate the locations where MT growth was observed.

(C) The directional distribution of MT growth in *fz* (green) and *stbm* (blue) mutants (see the legends of Figure 2B).

(D) The directional preference at 24 h APF [*: $p < 0.05$; Wilcoxon signed-rank test; actual p-values are 0.03574 (*fz*) and 0.019 (*stbm*)].

(E) Number of proximally shooting comets and that of distally shooting ones in each genotype at L3-1 at 24 h APF (see the legends of Figure 2D).

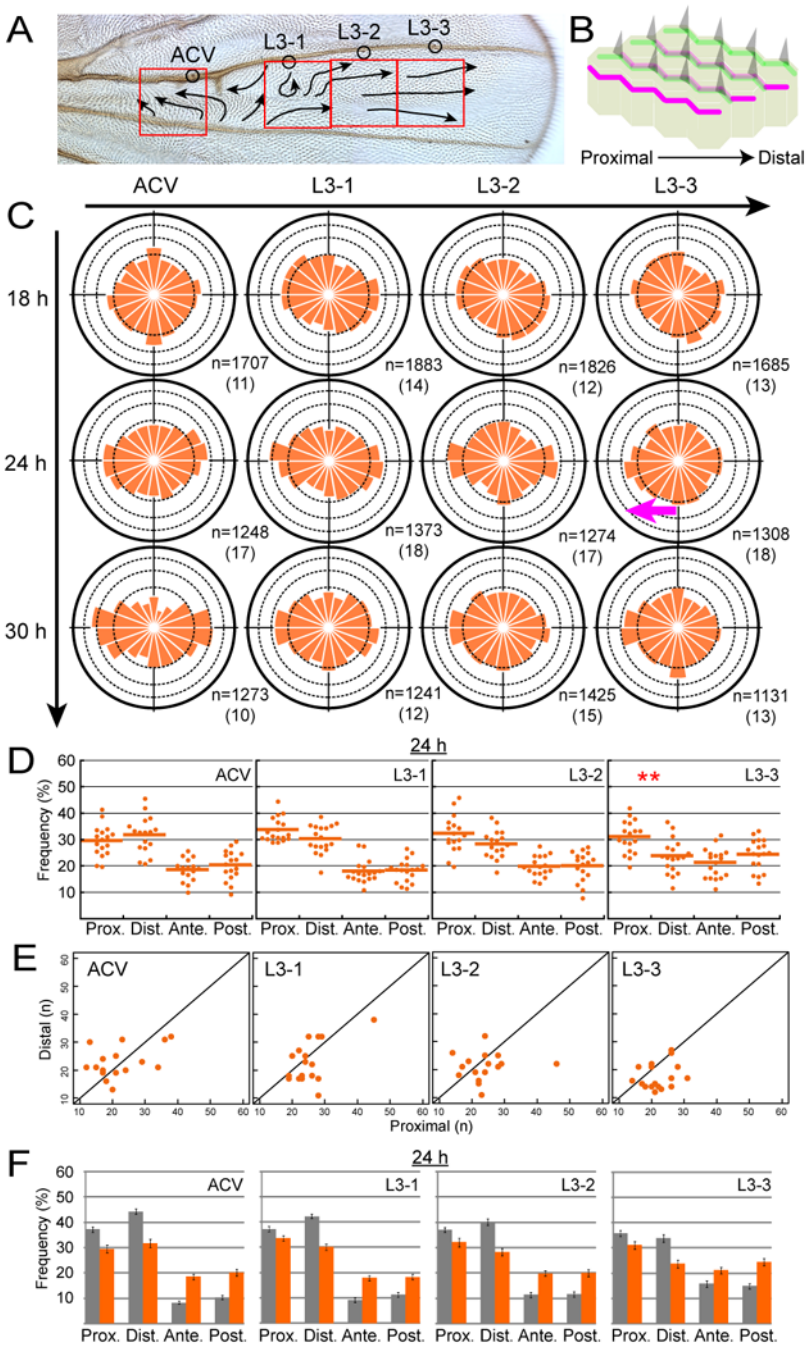

Figure 4. Abnormal MT dynamics in *ds* mutant wing

(A) Red boxes indicate 4 distinct locations observed in a *ds* mutant wing (see also Figure S1B). Arrows represent the hair polarity on the dorsal surface.

(B) Diagram of a small region in a *ds* mutant wing just after the onset of prehair formation. See details in the text.

(C) The directional distribution of MT growth in *ds* mutants. The magenta arrow indicates statistically significant asymmetry of MT polarity that was opposite to that in the wild-type wing at 24 h APF (Figure 2B; other explanations are in its legend).

(D) The directional preference at 24 h APF. + end-proximal MTs were more abundant than + end-distal ones at the distal L3-3 location (**: $p < 0.01$; Wilcoxon signed-rank test; actual p-value is 0.00599).
(E) Number of proximally shooting comets and that of distally shooting ones in each sample at each location at 24 h APF (see the Figure 2D legend).
(F) Comparisons of percentage of + ends in each direction between the wild type (gray bars) and *ds* mutant (orange bars) at 24 h APF. Each error bar indicates SEM. The directional preference was significantly different between the wild-type and the *ds* mutant wing at all of the locations examined ($p < 0.001$; Pearson's χ^2 test).

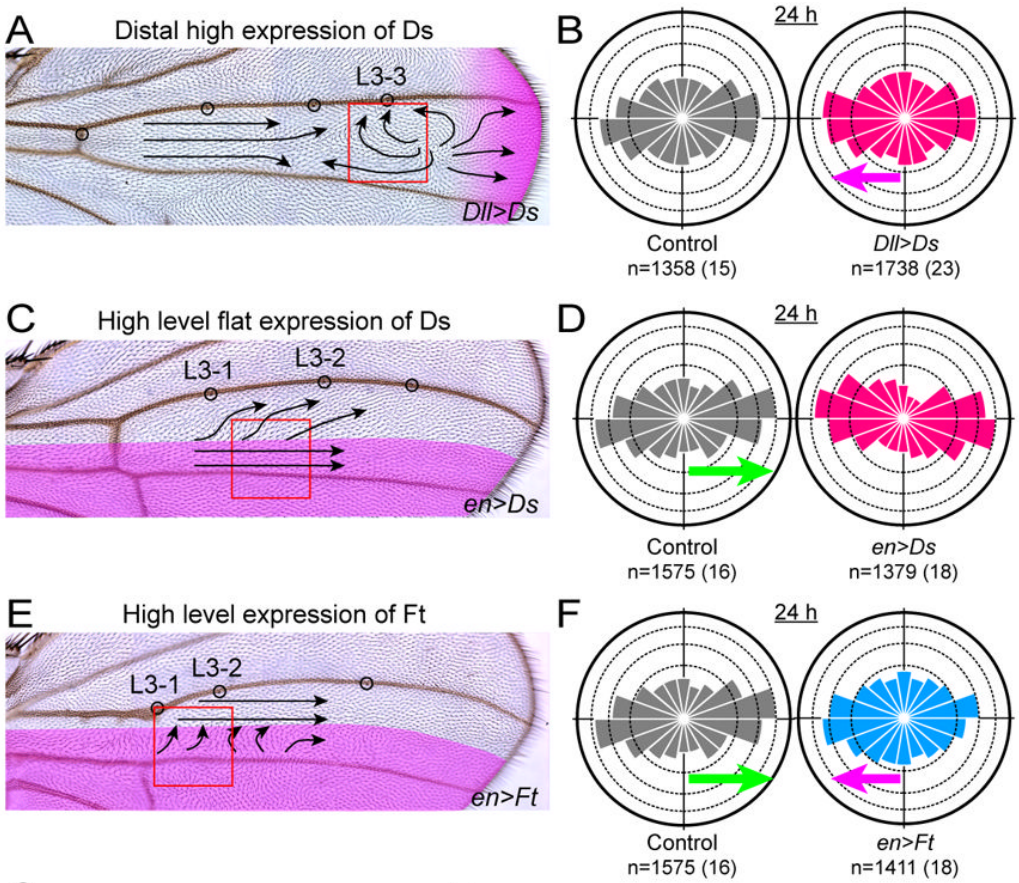

Figure 5. Effects of *ds* or *ft* misexpression on MT dynamics

(A, C, and E) Adult wings of animals in which *ds* or *ft* was misexpressed or overexpressed. The presumptive expression domains are shaded in magenta (see also Movies S5 and S6). Arrows represent the hair polarity on the dorsal surface. (A) *ds* was ectopically expressed in cells along the distal wing margin. (C and E) *ds* and *ft*, respectively were overexpressed in the posterior compartment.

(B, D, and F) MT growth at 24 h APF in the control animals (gray) and in the animals in "A," "C," and "E" (red and cyan, respectively). Green arrows, magenta arrows, and numbers below the diagrams are as explained in the legends of Figures 2B and 4C.

(G and H) The directional preference of EB1-GFP comets at 24 h APF at location L3-3 (G; red box in "A") and at the location between L3-1 and L3-2 (H; red boxes in "C" and "E"). Gray datum points were collected from the control animals, whereas red and cyan points

were from animals in “A,” ”C,” and “E,” respectively. Statistical significance of the directional preference between proximally oriented MTs and distally oriented MTs is indicated with asterisks (*: $p < 0.05$; **: $p < 0.01$; Wilcoxon signed-rank test). Actual p-values were 0.01614 (*Dll>Ds* in “G”), 0.01286 (control in “H”), and 0.003745 (*en>Ft* in “H”).

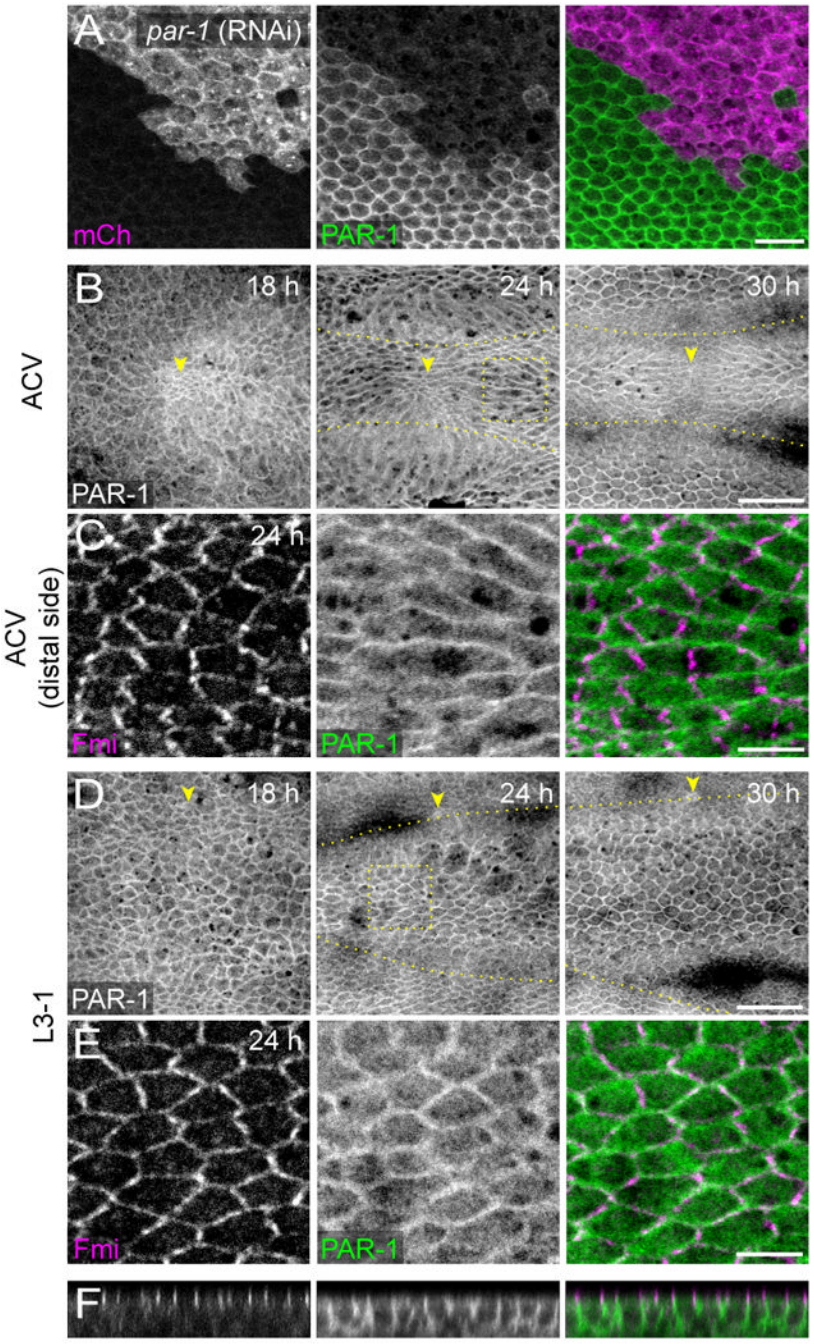

Figure 6. Subcellular localization of PAR-1 in the wild-type wing

(A) Specificity of our PAR-1 antibody in the wild-type wing (31 h APF). Cortical and cytoplasmic signals (green) were hardly detected in the clone that expressed *par-1* dsRNA and membrane-bound monomeric Cherry (mCherry-CAAX: magenta).

(B-E) ACV regions (B and C) and L3-1 regions (D and E) of 18 h, 24 h, and 30 h APF wings that were doubly stained for PAR-1 (B and D, and green in “C” and “E”) and Fmi (magenta in “C” and “E”). Arrowheads represent developing ACVs (B) and campaniform sensillum L3-1s (D). Dotted lines trace L3 and L4 veins. (C and E) High-power images of Fmi and PAR-1 patterns in the box in “B” and “D” are shown. On the right are the merged images of Fmi (magenta) and PAR-1 (green).

(F) A vertical section of a 30 h APF wing. Fmi (left), PAR-1 (middle), and a merged image of Fmi (magenta) and PAR-1 (green). Apical is at the top.
Bar scales: 10 μm (A), 20 μm (B and D), and 5 μm (C and E).

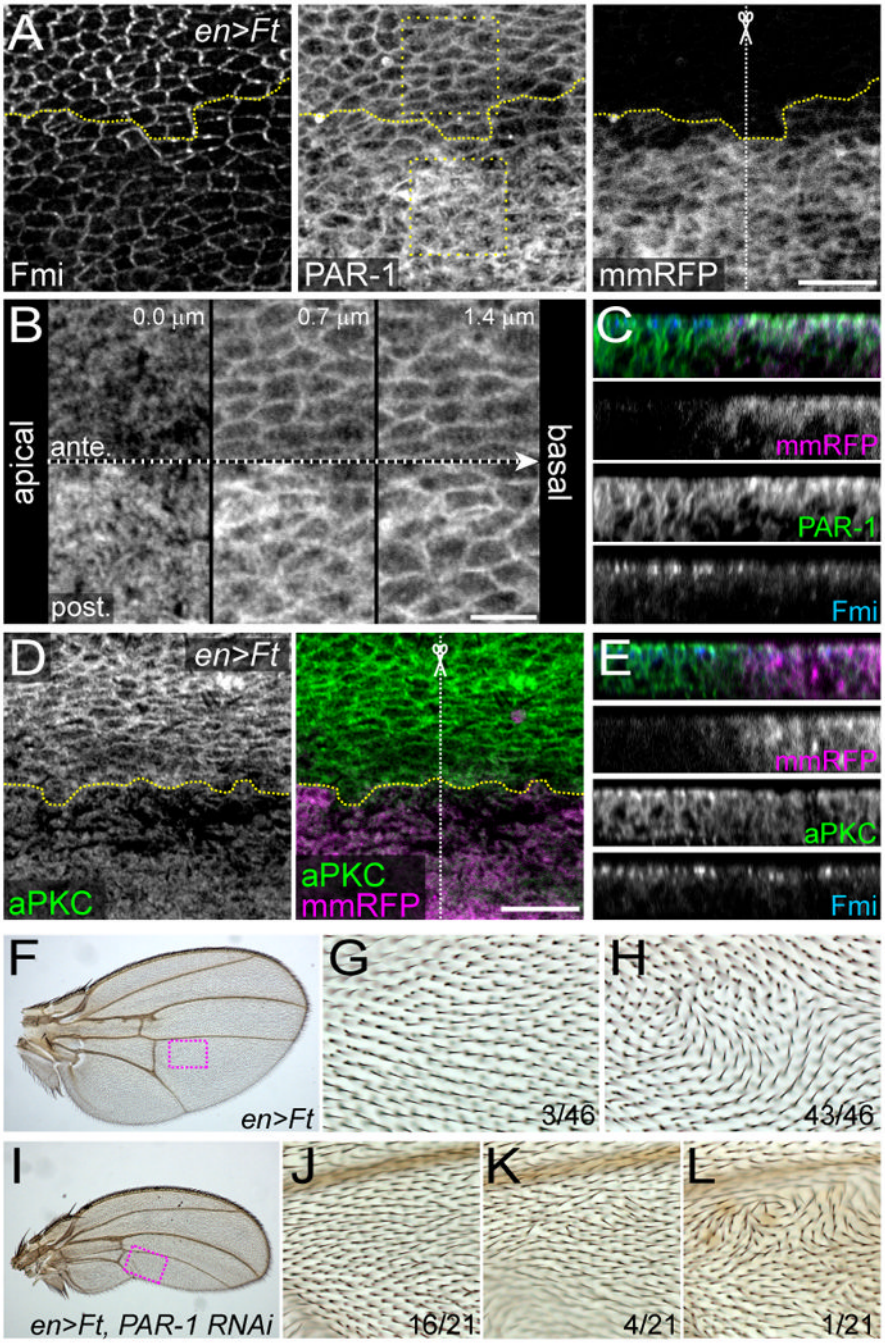

Figure 7. PAR-1 subcellular localization was altered when Ft was overexpressed

(A-C) *ft* was overexpressed in the posterior compartment (*en>Ft*) and stained for Fmi (left) and PAR-1 (middle) at 24 h APF (A). The posterior compartment was labeled by mmRFP (right), and the dotted yellow lines demarcate borders of the expression domain. All panels are projections of 5 optical sections. High-power images of the 2 boxed regions in anterior and posterior compartments are shown on the top (ante.) and at the bottom (post.), respectively, in "B." The images were taken from apical (left) to basal (right) at 0.7-μm intervals. The z section along the dotted white line marked by the scissor in "A" is shown in "C," which includes a merge and single-channel images for mmRFP (magenta), PAR-1 (green), and Fmi (blue).

(D and E) An *en>Ft* wing at 24 h APF was stained for aPKC (green in “D” and “E”) and Fmi (blue in “E”). The expression domain was labeled by mmRFP (magenta), and dotted yellow lines demarcate the borders of the domains. The z section along the dotted white line in “D” is shown in “E,” which includes a merge and single-channel images for mmRFP (magenta), aPKC (green), and Fmi (blue).
Bar scales: 10 μm (A and D), 5 μm (B).
(F-L) Adult wings of animals in which *ft* (F-H) or *ft* and *PAR-1 dsRNA* (I-L) were overexpressed in the posterior compartment of the wing. *ft* overexpression caused a highly-penetrant polarity phenotype (G and H; boxed region in “F”), which was suppressed when *par-1* was knocked down (J-L; boxed region in “I”). All of the 21 knocked-down wings examined had a similar size.

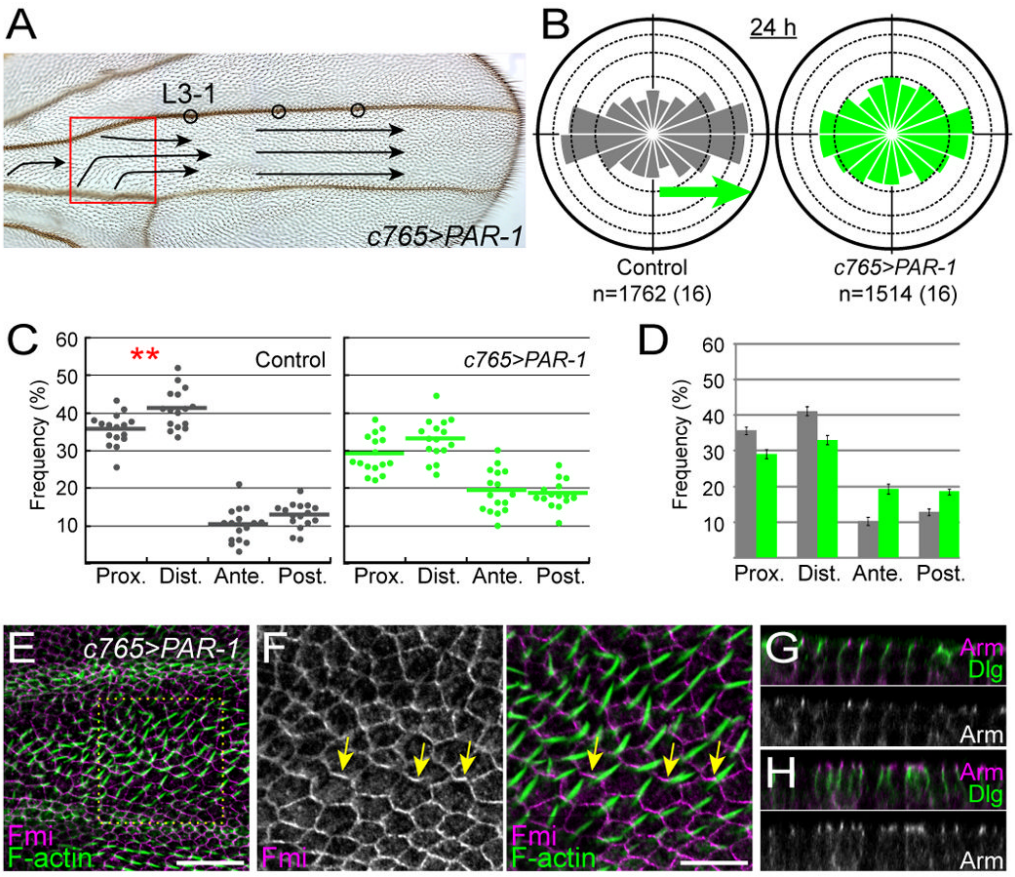

Figure 8. *par-1* overexpression disrupted PCP and the MT dynamics at the proximal location

(A) The red box indicates the location where we observed MT growth in a *par-1*-overexpressing wing (*c765>PAR-1*). Arrows represent the hair polarity in region C (see Figure 1A) on the dorsal surface.

(B) The directional distribution of MT growth at 24 h APF in the control wing (gray) and the *par-1*-overexpressing wing (green). The green arrow and numbers below the diagrams are as explained in the legends of Figure 2B.

(C) The directional preference of the EB1-GFP comets at 24 h APF, at a location between ACV and L3-1 in the control wing (gray data points), and at the boxed location in "A" in the *par-1*-overexpressing wing (green datum points). Statistical significance of differences between proximally oriented MTs and distally oriented MTs are indicated with an asterisk (**: $p < 0.01$; Wilcoxon signed-rank test). The actual p-value was 0.004855 (control).

(D) Statistical comparisons of frequency of + ends in each direction between the wild-type (gray) and the *par-1*-overexpressing wing (green) at 24 h APF. Each error bar indicates SEM. The directional preference was significantly different between the wild-type and the *par-1*-overexpressing wing ($p < 0.001$; Pearson's χ^2 test).

(E and F) 33 h APF wing that was doubly stained for Fmi (magenta) and F-actin (green). The imaged location corresponds to the red box in "A." High-power image of the box in "E" is highlighted in "F." Fmi was tightly associated with cell boundaries including A/P boundaries (arrows). Wing hairs (green) were generated at cell vertexes that were connected to those Fmi-mislocalized A/P boundaries.

(G and H) Vertical sections of 33 h APF wings of a control animal (G) and a *par-1*-overexpressing one (H) that were doubly labeled for apically localized Armadillo (Arm; magenta) and basolaterally located Discs-large (Dlg; green). Apical is at the top.

Bar scales: 20 μm (E) and 10 μm (F).